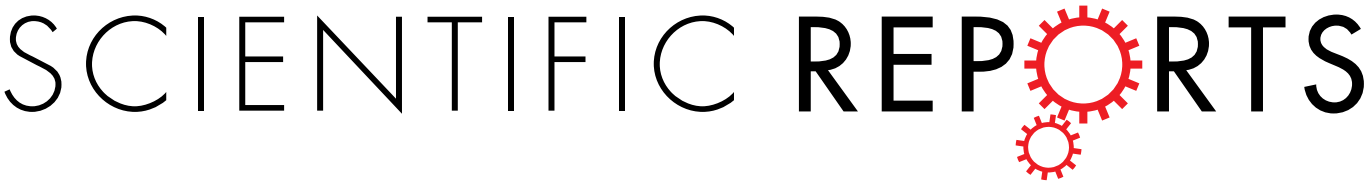

OPEN

Structures, stabilities and spectral properties of borospherene B_{44}^- and metalloborospherenes $MB_{44}^{0/-}$ (M = Li, Na, and K)

Received: 03 October 2016
Accepted: 30 November 2016
Published: 10 January 2017

Shixiong Li[1,2], Zhengping Zhang[1], Zhengwen Long[3] & Shuijie Qin[4]

Density functional theory (DFT) and time-dependent density functional theory (TD-DFT) calculations are carried out to study the stabilities, photoelectron, infrared, Raman and electronic absorption spectra of borospherene B_{44}^- and metalloborospherenes $MB_{44}^{0/-}$ (M = Li, Na, and K). It is found that all atoms can form stable exohedral metalloborospherenes $M\&B_{44}^{0/-}$, whereas only Na and K atoms can be stably encapsulated inside $B_{44}^{0/-}$ cage. In addition, relative energies of these metalloborospherenes suggest that Na and K atoms favor exohedral configuration. Importantly, doping of metal atom can modify the stabilities of B_{44} with different structures, which provides a possible route to produce stable boron clusters or metalloborospherenes. The calculated results suggest that B_{44} tends to get electrons from the doped metal. Metalloborospherenes MB_{44}^- are characterized as charge-transfer complexes ($M^{2+}B_{44}^{2-}$), where B_{44} tends to get two electrons from the extra electron and the doped metal, resulting in similar features with anionic B_{44}^{2-}. In addition, doping of metal atom can change the spectral features, such as blueshift or redshift and weakening or strengthening of characteristic peaks, since the extra metal atom can modify the electronic structure. The calculated spectra are readily compared with future spectroscopy measurements and can be used as fingerprints to identify B_{44}^- and metalloborospherenes.

Discovery of fullerene C_{60} is an important milestone in chemistry and materials science and leads to nowadays popular carbon-based nanomaterials such as carbon nanotubes and graphenes[1–4]. Fullerene C_{60} is spherical carbon cluster with a hollow cavity, which can encapsulate ion, atom or molecule inside the cage such as $M@C_{60}$ (M = Li, N, H_2, N_2, and H_2O) and $M^+@C_{60}$ (M = Li, H, Na, and K)[5–11]. These fullerene derivatives are known as endofullerenes which can produce new properties or improve the existing properties of fullerene C_{60}. These endofullerenes based on C_{60} have attracted much attention due to their potential applications in materials science. Although boron is neighbor of carbon, boron is an electron deficient atom with only three valence electrons. Experimental and theoretical works have shown that most boron clusters are planar or quasi-planar structures[12–19] before the intriguing fullerene-like cluster B_{80} predicted in 2007[20]. Subsequently, fullerene-like B_{80} was found not to be the global minimum, and the most favorable B_{80} is likely a core-shell type three-dimensional structure[21,22]. Since the first proposal of a possible B_{80} cage, the pursuit of all-boron fullerenes has attracted significant computational activities in the past several years[23–28]. Nevertheless, there has been no experimental evidence of the existence of all-boron fullerene in the past several decades.

An all-boron fullerene-like cluster B_{40}^- and quasi-planar cluster B_{40}^- were produced in a laser vaporization supersonic source in 2014[29]. Relevant theoretical simulations indicated that cage B_{40}^- is slightly less stable than the quasi-planar global minimum B_{40}^-, however, neutral cage cluster B_{40} is the most stable structure among the isomers of B_{40}. Photoelectron spectroscopy analysis indicated that combination of the simulated photoelectron spectra of cage B_{40}^- and quasi-planar B_{40}^- can reproduce the observed spectrum, which confirmed the existence of cage B_{40}^-. Soon after, the cage cluster B_{39}^- was also produced via laser vaporization[30]. The first observation of

[1]College of Big Data and Information Engineering, Guizhou University, Guiyang 550025, China. [2]School of Physics and Electronic Science, Guizhou Education University, Guiyang 550018, China. [3]College of Science, Guizhou University, Guiyang 550025, China. [4]Key Lab of Photoelectron Technology and Application, Guizhou University, Guiyang 550025, China. Correspondence and requests for materials should be addressed to S.L. (email: leesxoptics@163.com) or Z.Z. (email: zpzhang@gzu.edu.cn)

the borospherene has aroused interest in all-boron fullerenes and their derivatives such as dynamical behavior of B_{40}[31], hydrogen storage capacity of Ti-decorated B_{40}[32], experimental and theoretical studies of B_{28}^- and B_{29}^- borospherenes[33,34], structures and electronic properties of metalloborospherenes (Ca@B_{40}, Be&B_{40}, Sc@B_{40}, Li&B_{40}, Na@B_{40}, Ca@B_{39}^+, Ca@B_{38}, Ca@B_{37}^- and Li_4&B_{36})[35–41], and spectral properties of borospherenes[42,43].

Recently, a new borospherene B_{44} was reported[44], relevant theoretical simulations indicated that neutral cage cluster B_{44} containing two nonagonal, two hexagonal and two heptagonal holes is the most stable structure among the isomers of B_{44}. In addition, energies of first five lowest-lying isomers are close to each other, it is possible to expect that the five isomers may appear in the future experiments. It is necessary to study the structures and spectral characteristics of anionic B_{44}^- and metalloborospherenes $MB_{44}^{0/-}$ (M = Li, Na, and K). The structure search algorithms and DFT combined approaches have been used and the low-lying structures of boron clusters have been reported by many authors[26,28–30,44]. It is not our purpose in this work to carry out an extensive structure search for the global minimum of B_{44}^- cluster and metalloborospherenes $MB_{44}^{0/-}$ (M = Li, Na, and K). Instead, we will collect the B_{44} structures from the paper (*Chem. Commun.*, 2016, 52, 1653–1656) and study the structures, stabilities of corresponding anionic B_{44}^- and metalloborospherenes $MB_{44}^{0/-}$ (M = Li, Na, and K). Current works are therefore to provide a theoretical study on the stabilities, photoelectron spectra, infrared, Raman and electronic absorption spectra of B_{44}^- and metalloborospherenes $MB_{44}^{0/-}$ (M = Li, Na, and K). Our works may provide valuable results to assist further experimental identifications on the borospherene B_{44}^- and metalloborospherenes $MB_{44}^{0/-}$ (M = Li, Na, and K), and also may provide theoretical guidance for the applications and synthesis of them in the future.

To obtain the adiabatic detachment energy (ADE) and contrastive analysis, the five lowest-lying neutral isomers of B_{44} reported by Tai *et al.*[44] were re-optimized using the density functional method PBE0 with 6–311 + G* basis set. The five corresponding anionic isomers were optimized using the DFT functionals TPSSh and PBE0 in conjunction with the 6–311 + G* basis set. To obtain more accurate relative energies, single-point electronic energies of the five anionic isomers were subsequently calculated using the coupled-cluster theory UCCSD(T)/3–21 G method at their PBE0/6–311 + G* optimized geometries. All ground-state geometries of the metalloborospherenes $MB_{44}^{0/-}$ and frequency calculations were performed based on the density functional method PBE0 with 6–311 + G* basis set. These optimized structures were then used in the calculations of photoelectron spectra and electronic absorption spectra based on the time-dependent DFT formalism[45] at the same level. All computations were carried out using the Gaussian09 software package[46].

Results and Discussion

Optimized structures of borospherenes $B_{44}^{0/-}$ are depicted in Fig. 1. Ground-state parameters are summarized in Table 1. Frequency calculations confirm the stability of $B_{44}^{0/-}$ by showing no imaginary frequencies. The relative energy values of neutral B_{44} agree well with the results of Tai *et al.*[44] that isomer **IV** is the most stable form and isomer **I** is the third stable form. However, our TPSSh, PBE0 and UCCSD(T) energy values of anionic B_{44}^- indicate that isomer **I** is the most stable form of the five isomers. Although the neutral isomer **II** and isomer **III** have different structures[44] (isomer **II** includes two octagonal B_8, two heptagonal B_7 and two hexagonal B_6 holes, isomer **III** includes two octagonal B_8, three heptagonal B_7 and one hexagonal B_6 holes), optimized structures of anionic isomer **II** and **III** show that the two isomers have almost the same structure (two octagonal B_8, two heptagonal B_7 and two hexagonal B_6 holes). It suggests that the two neutral isomers have the similar structures (only have a very small difference). In addition, for the sake of contrastive analysis, we also study the dianion B_{44}^{2-} (**I** and **IV**), ground-state parameters are summarized in Table S1. The relative energy values of dianion B_{44}^{2-} indicate that B_{44}^{2-} (**I**) is more stable than B_{44}^{2-} (**IV**). Interestingly, isomer **I** is quite similar to cage B_{40} and includes two octagonal, four heptagonal and one hexagonal holes, it can be constructed by replacing two opposite heptagonal holes of the borospherene B_{40} by two octagonal holes and splitting one hexagonal hole of the B_{40} into two neighbouring heptagonal holes. We will focus on the two isomers (**I** and **IV**) and corresponding metalloborospherenes $MB_{44}^{0/-}$ (M = Li, Na, and K).

Optimized structures of metalloborospherenes $MB_{44}^{0/-}$ (M = Li, Na, and K) are depicted in Figure S1 (Supplementary Information). Ground-state parameters are summarized in Table 2. Frequency calculations confirm the stability of these endohedral and exohedral metalloborospherenes (except for endohedral Li@$B_{44}^{0/-}$) by showing no imaginary frequencies. Endohedral Li@$B_{44}^{0/-}$ (**I**) and Li@$B_{44}^{0/-}$ (**IV**) prove to be unstable with imaginary frequencies. The calculated results indicate that Na atoms in Na@B_{44}^- (**I**), Na@B_{44} (**I**), Na@B_{44}^- (**IV**) and Na@B_{44} (**IV**) are slightly off the molecular center by 0.14, 0.11, 1.28 and 1.18 Å, respectively, along the C_2 molecular axis. In addition, K atoms in K@B_{44}^- (**I**), K@B_{44} (**I**), K@B_{44}^- (**IV**) and K@B_{44} (**IV**) are slightly off the molecular center by 0.12, 0.11, 0.09 and 0.04 Å, respectively, along the C_2 molecular axis. Energies of these metalloborospherenes $MB_{44}^{0/-}$ (M = Na and K) indicate that most endohedral metalloborospherenes M@$B_{44}^{0/-}$ (M = Na and K) are less stable than corresponding exohedral metalloborospherenes M&$B_{44}^{0/-}$ (M = Na and K), respectively, whereas only the exohedral Na&B_{44}^- (**IV**) is less stable than endohedral Na@B_{44}^- (**IV**). The results reveal that Li, Na and K atoms favor the exohedral configuration. It's worth noting that the energy differences between the endohedral metalloborospherenes M@$B_{44}^{0/-}$ (M = Na, K) and corresponding exohedral metalloborospherenes M&$B_{44}^{0/-}$ (M = Na, K) are small. Interestingly and encouragingly, although B_{44} (**I**) is less stable than B_{44} (**IV**), Table 2 shows that Li&B_{44} (**IV**), Na&B_{44} (**IV**), Na@B_{44} (**IV**), K&B_{44} (**IV**) and K@B_{44} (**IV**) are less stable than corresponding Li&B_{44} (**I**), Na&B_{44} (**I**), Na@B_{44} (**I**), K&B_{44} (**I**) and K@B_{44} (**I**), respectively, the addition of metal atom enhances the stability of isomer **I** compared with isomer **IV**. The results may provide a possible route (doping of metal atoms) to produce stable borospherenes or metalloborospherenes which have good properties and potential applications.

Photoelectron spectroscopy is powerful experimental technique to probe the electronic structure of cluster. It can be viewed as an electronic fingerprint for the underlying cluster. Photoelectron spectroscopy in combination with theoretical calculations has been used to understand and identify the structures of size-selected

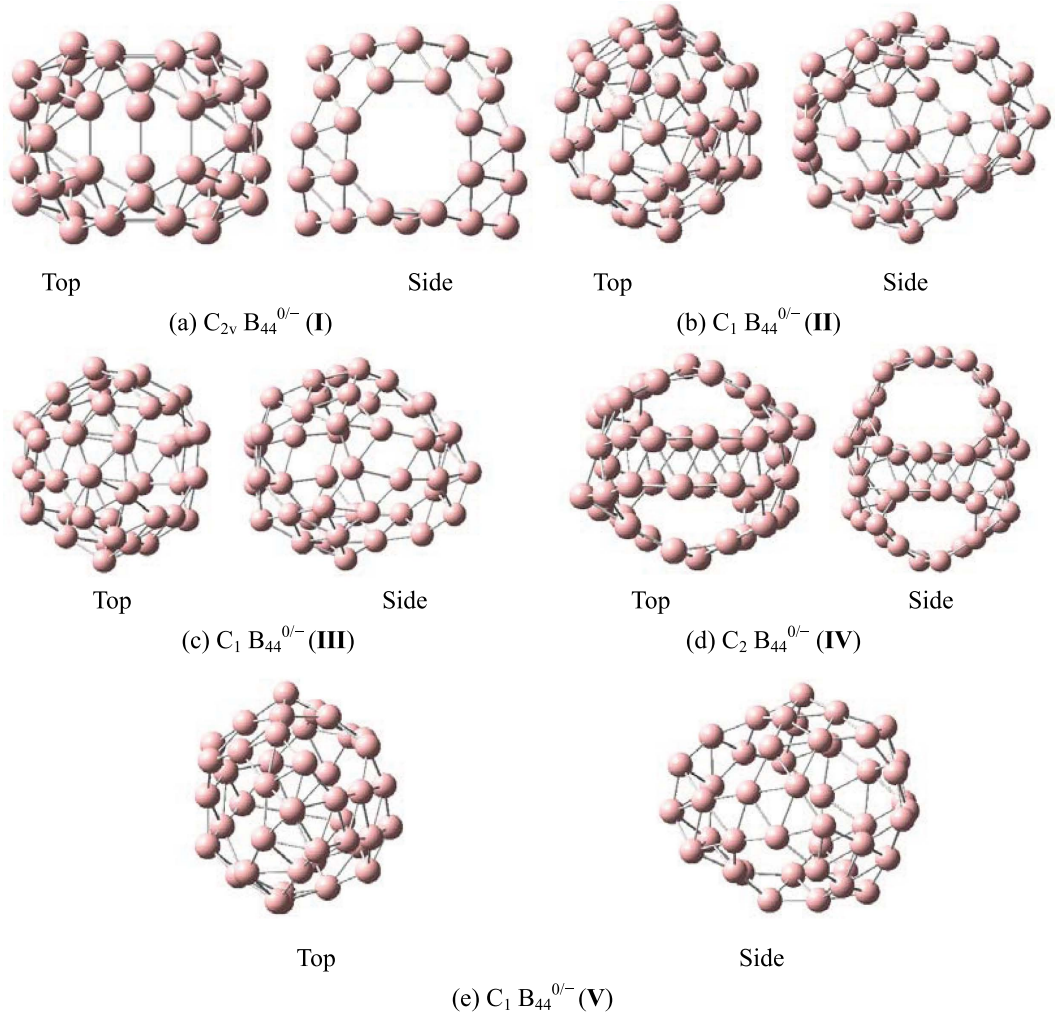

Figure 1. Optimized Structures for the five isomers of $B_{44}^{0/-}$ at the PBE0/6–311 + G* level.

boron clusters[29,30]. To facilitate future identifications of B_{44}^-, the ADEs for B_{44}^- and metalloborospherenes MB_{44}^- (M = Li, Na, and K) were calculated at the PBE0 level, then we calculated the vertical detachment energies (VDEs) and simulated the photoelectron spectra for B_{44}^- and metalloborospherenes MB_{44}^- (M = Li, Na, and K), using the time-dependent DFT (TD-DFT) method[29,30,45]. Adiabatic detachment energy of B_{44}^- represents the electron affinity (EA) of corresponding neutral B_{44}. The larger EA can lead to the stronger probability of capturing an electron, i.e., the neutral B_{44} with larger EA is easier to capture an electron. The five isomers give the ground-state ADEs of 3.23(**I**), 3.02(**II**), 3.02(**III**), 2.78(**IV**) and 2.99(**V**) eV, respectively. Among the five isomers of B_{44}^-, isomer **I** has the largest ADE (3.23 eV), which is larger than the ADE (2.29 eV)[29] of cage B_{40}^- and less than the ADE (3.51 eV)[29] of quasi-planar B_{40}^-. The calculated ground-state ADEs of Li&B_{44}^- (**I**), Li&B_{44}^- (**IV**), Na&B_{44}^- (**I**), Na&B_{44}^- (**IV**), Na@B_{44}^- (**I**), Na@B_{44}^- (**IV**), K&B_{44}^- (**I**), K&B_{44}^- (**IV**), K@B_{44}^- (**I**) and K@B_{44}^- (**IV**) are 3.17, 2.96, 3.01, 2.79, 3.24, 3.11, 2.87, 2.63, 3.22 and 3.01 eV, respectively. The calculated results indicate that doping of alkali metal atom in B_{44}^- (**I**) can decrease the ADE of B_{44}^- (**I**), however, doping of alkali metal atom in B_{44}^- (**IV**) can increase the ADE of B_{44}^- (**IV**).

Photoelectron spectra of five isomers are given in Fig. 2. The predicted photoelectron spectra show that isomer **IV** has the lowest first vertical detachment energy (VDE) and the largest energy gap (about 0.73 eV) between the first and second bands. The first several bands of photoelectron spectra were used to identify boron clusters[29,30], so we will focus on the bands at the low binding energy side. The first peaks of five isomers come from the calculated ground-state VDEs at 3.34(**I**), 3.19(**II**), 3.19(**III**), 2.95(**IV**) and 3.38(**V**) eV, respectively. The calculated ground-state VDE of each isomer originates from the detachment of the electron from the singly occupied molecular orbital (α-SOMO). The second peaks of the five isomers come from the second calculated VDEs at 3.48(**I**), 3.56(**II**), 3.56(**III**), 3.68(**IV**) and 3.72(**V**) eV, respectively. The second calculated VDEs of five isomers originate from detaching the electron from β-HOMO-1 resulting in the first triplet state. Figure 2(b,c) indicate that isomer **II** and isomer **III** have the same photoelectron spectrum, which confirms that the two isomers have almost the same structure.

Figure 3 presents the photoelectron spectra of metalloborospherenes MB_{44}^- (M = Li, Na, and K). The first peaks of the photoelectron spectra come from the calculated ground-state VDEs of Li&B_{44}^- (**I**), Li&B_{44}^- (**IV**), Na&B_{44}^- (**I**), Na&B_{44}^- (**IV**), Na@B_{44}^- (**I**), Na@B_{44}^- (**IV**), K&B_{44}^- (**I**), K&B_{44}^- (**IV**), K@B_{44}^- (**I**) and K@B_{44}^- (**IV**)

	Isomer	Symmetry	*E*/hartree	relative energy/eV	E_g/eV	μ/Debye	State
B_{44}	**I**	C_{2v}	−1091.8943	0.17	1.3524	2.0800	$^1A_1$
B_{44}	**II**	C_1	−1091.8956	0.14	1.8515	1.3011	^1A
B_{44}	**III**	C_1	−1091.8955	0.14	2.2410	1.6519	^1A
B_{44}	**IV**	C_2	−1091.9007	0.00	2.1205	0.9490	^1A
B_{44}	**V**	C_1	−1091.8920	0.24	2.5946	1.7655	^1A
B_{44}^-	**I**	C_{2v}	−1092.0129	0.00	1.9769[a]	2.5928	$^2A_2$
			−1093.6775[c]	[0.00]	1.2716[b]		
			−1081.8145[d]	(0.00)			
B_{44}^-	**II**	C_1	−1092.0068	0.17	2.1088[a]	2.5478	^2A
			−1093.6719[c]	[0.15]	1.9092[b]		
			−1081.7928[d]	(0.59)			
B_{44}^-	**III**	C_1	−1092.0068	0.17	1.9628[a]	2.5600	^2A
			−1093.6719[c]	[0.15]	1.9078[b]		
			−1081.7928[d]	(0.59)			
B_{44}^-	**IV**	C_2	−1092.0028	0.27	1.4938[a]	2.1723	^2A
			−1093.6688[c]	[0.24]	1.9168[b]		
			−1081.7963[d]	(0.50)			
B_{44}^-	**V**	C_1	−1092.0021	0.29	2.0737[a]	3.9325	^2A
			−1093.6682[c]	[0.25]	2.2908[b]		
			−1081.7925[d]	(0.60)			

Table 1. The symmetries, energies (*E*), relative energies (neutral B_{44}: the energy of B_{44} (IV) is set to be zero, anionic B_{44}^-: the energy of B_{44}^- (I) is set to be zero), energy gaps (E_g), dipole moments (μ) and states of borospherenes $B_{44}^{0/-}$ optimized at PBE0/6–311 + G* level. The superscripts a and b denote the alpha electron and beta electron, respectively. The superscripts c and d denote the energies (*E*) of B_{44}^- at TPSSh/6–311 + G* and UCCSD(T)/3–21 G//PBE0/6–311 + G* levels. The square bracket and round bracket denote the relative energies of B_{44}^- at TPSSh/6–311 + G* and UCCSD(T)/3–21 G//PBE0/6–311 + G* levels.

$MB_{44}^{0/-}$	B_{44} structure	Symmetry	*E*/hartree	relative energy/eV	E_g/eV	μ/Debye	State
Li&B_{44}	**I**	C_s	−1099.4814	(3.17)	2.0305[a], 1.6228[b]	2.6775	^2A”
Na&B_{44}	**I**	C_s	−1254.1542	[3.01]	2.0193[a], 1.5917[b]	5.9058	^2A”
Na@B_{44}	**I**	C_{2v}	−1254.1450	[3.26]	1.8545[a], 1.3614[b]	2.4171	$^2A_2$
K&B_{44}	**I**	C_s	−1691.7302	{2.87}	2.0196[a], 1.5711[b]	8.9039	^2A”
K@B_{44}	**I**	C_{2v}	−1691.7140	{3.31}	1.8537[a], 1.3461[b]	2.4406	$^2A_2$
Li&B_{44}^-	**I**	C_s	−1099.5978	(0.00)	1.9491	4.3131	^1A’
Na&B_{44}^-	**I**	C_s	−1254.2647	[0.00]	1.9357	7.7502	^1A’
Na@B_{44}^-	**I**	C_{2v}	−1254.2640	[0.02]	1.8848	3.0687	$^1A_1$
K&B_{44}^-	**I**	C_s	−1691.8357	{0.00}	1.9491	11.1740	^1A’
K@B_{44}^-	**I**	C_{2v}	−1691.8325	{0.09}	1.8832	3.0501	$^1A_1$
Li&B_{44}	**IV**	C_1	−1099.4726	(3.41)	1.6793[a], 2.0169[b]	1.7322	^2A
Na&B_{44}	**IV**	C_1	−1254.1494	[3.14]	1.6611[a], 2.0449[b]	4.9882	^2A
Na@B_{44}	**IV**	C_2	−1254.1427	[3.32]	1.6587[a], 1.7887[b]	1.0043	^2A
K&B_{44}	**IV**	C_1	−1691.7234	{3.06}	1.6426[a], 2.0335[b]	8.1784	^2A
K@B_{44}	**IV**	C_2	−1691.7009	{3.67}	1.4884[a], 1.8346[b]	1.8479	^2A
Li&B_{44}^-	**IV**	C_1	−1099.5813	(0.45)	1.7096	1.7304	^1A
Na&B_{44}^-	**IV**	C_1	−1254.2518	[0.35]	1.7009	4.2752	^1A
Na@B_{44}^-	**IV**	C_2	−1254.2569	[0.21]	1.6819	1.9305	^1A
K&B_{44}^-	**IV**	C_1	−1691.8202	{0.42}	1.6824	7.7875	^1A
K@B_{44}^-	**IV**	C_2	−1691.8116	{0.66}	1.5668	2.9593	^1A

Table 2. The symmetries, energies (*E*), relative energies (the round bracket denotes the relative energies of $LiB_{44}^{0/-}$ and the energy of Li&B_{44}^- (I) is set to be zero; the square bracket denotes the relative energies of $NaB_{44}^{0/-}$ and the energy of Na&B_{44}^- (I) is set to be zero; the curly bracket denotes the relative energies of $KB_{44}^{0/-}$ and the energy of K&B_{44}^- (I) is set to be zero), energy gaps (E_g), dipole moments (μ) and states of metalloborospherenes $MB_{44}^{0/-}$ (M = Li, Na, and K) optimized at PBE0/6–311 + G* level. The superscripts a and b denote the alpha electron and beta electron, respectively.

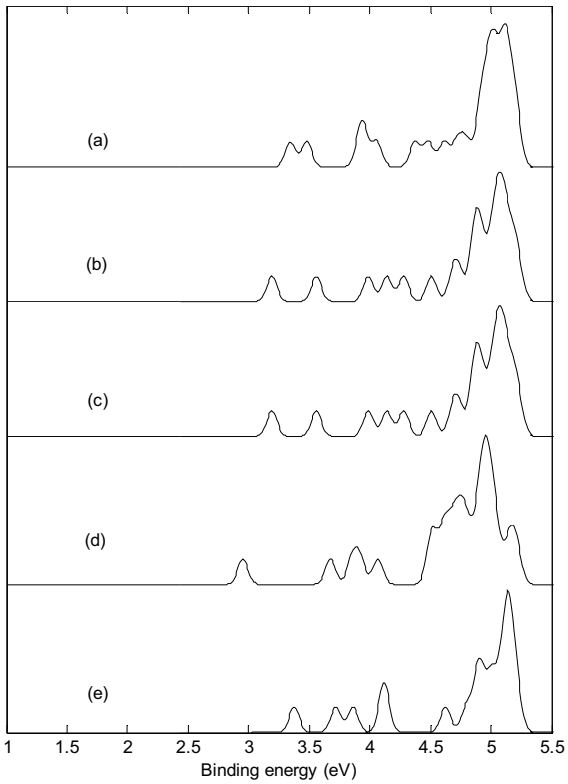

Figure 2. Simulated photoelectron spectra for the 5 isomers of B_{44}^- based on PBE0 functional with 6–311 + G* basis set. (**a**): C_{2v} B_{44}^- (**I**), (**b**): C_1 B_{44}^- (**II**), (**c**): C_1 B_{44}^- (**III**), (**d**): C_2 B_{44}^- (**IV**), (**e**): C_1 B_{44}^- (**V**). The simulations were done by fitting the distributions of calculated vertical detachment energies at the PBE0 level with unit-area Gaussian functions of 0.05 eV half-width.

at 3.32, 3.11, 3.17, 2.95, 3.34, 3.23, 3.03, 2.70, 3.32 and 3.15 eV, respectively. The calculated ground-state VDEs of metalloborospherenes originate from the detachment of the electron from the molecular orbital (HOMO). The predicted photoelectron spectra in Fig. 3 show that the first VDEs of Li&B_{44}^- (**I**), Na&B_{44}^- (**I**), K&B_{44}^- (**I**), Na@B_{44}^- (**I**) and K@B_{44}^- (**I**) are lager than that of Li&B_{44}^- (**IV**), Na&B_{44}^- (**IV**), K&B_{44}^- (**IV**), Na@B_{44}^- (**IV**) and K@B_{44}^- (**IV**), respectively. The second peaks of Li&B_{44}^- (**I**), Na&B_{44}^- (**I**), Na@B_{44}^- (**I**), Na@B_{44}^- (**IV**), K&B_{44}^- (**I**), K@B_{44}^- (**I**) and K@B_{44}^- (**IV**) come from the second calculated VDEs at 3.84, 3.66, 3.75, 3.82, 3.51, 3.72 and 3.76 eV, respectively. The second calculated VDEs of metalloborospherenes originate from detaching the electron from HOMO-1. The second peaks of Li&B_{44}^- (**IV**), Na&B_{44}^- (**IV**) and K&B_{44}^- (**IV**) come from the second and third calculated VDEs, interestingly, the second and third calculated VDEs of each metalloborospherene (Li&B_{44}^- (**IV**), Na&B_{44}^- (**IV**) or K&B_{44}^- (**IV**)) are almost overlapped and correspond to an electron detachment from the HOMO-1 and HOMO-2 (orbital energies of HOMO-1 and HOMO-2 are almost degenerate). Figure 3(a,c,g) indicate that exohedral Li&B_{44}^- (**I**), Na&B_{44}^- (**I**) and K&B_{44}^- (**I**) have the similar spectral features, however, all bands move to lower binding energy side with the increase of radius of doped atom. Similarly, exohedral Li&B_{44}^- (**IV**), Na&B_{44}^- (**IV**) and K&B_{44}^- (**IV**) also have such characteristics. The simulated photoelectron spectrum of Na@B_{44}^- (**IV**) is somewhat similar to the spectrum of Na@B_{44}^- (**I**), whereas the third peak of Na@B_{44}^- (**IV**) can be used to distinguish the Na@B_{44}^- (**I**) and Na@B_{44}^- (**IV**). Figure 3(e,i) indicate that simulated photoelectron spectra of Na@B_{44}^- (**I**) and K@B_{44}^- (**I**) have the similar spectral features, particularly, the first three peaks are almost same. Figure 3 indicate that photoelectron spectra of Li&B_{44}^- (**I**), Na&B_{44}^- (**I**), K&B_{44}^- (**I**), Na@B_{44}^- (**I**) and K@B_{44}^- (**I**) are different from that of Li&B_{44}^- (**IV**), Na&B_{44}^- (**IV**), K&B_{44}^- (**IV**), Na@B_{44}^- (**IV**) and K@B_{44}^- (**IV**), respectively. These features can be used to distinguish the metalloborospherenes MB_{44}^- (**I**) and metalloborospherenes MB_{44}^- (**IV**).

Figures 2(a,d) and 3 indicate that the addition of alkali metal atom modifies the photoelectron spectra of B_{44}^- since the addition of extra atom modifies the electronic structure. The calculated results indicate that doping of alkali metal atom in B_{44}^- (**I**) can decrease the first VDE of B_{44}^- (**I**), however, doping of alkali metal atom in B_{44}^- (**IV**) can increase the first VDE of B_{44}^- (**IV**). The predicted photoelectron spectra in Figs 2 and 3 show that B_{44}^- and metalloborospherenes MB_{44}^- (M = Li, Na, and K) have different spectral features, the predicted photoelectron spectra provide important information for the identification of B_{44}^- and metalloborospherenes MB_{44}^- (M = Li, Na, and K). It is worth to note that the structures of atomic clusters cannot directly be identified by common analytical expermenttal methods, but they can indirectly be determined by using combined theoretical and experimental studies. As the discovery of B_{40}, if the photoelectron spectra of B_{44}^- and metalloborospherenes MB_{44}^- (M = Li, Na, and K) are obtained in experiments, these calculated characteristic bands may be used as theoretical basis for the identification of boron cluster B_{44}^- and metalloborospherenes MB_{44}^- (M = Li, Na, and K).

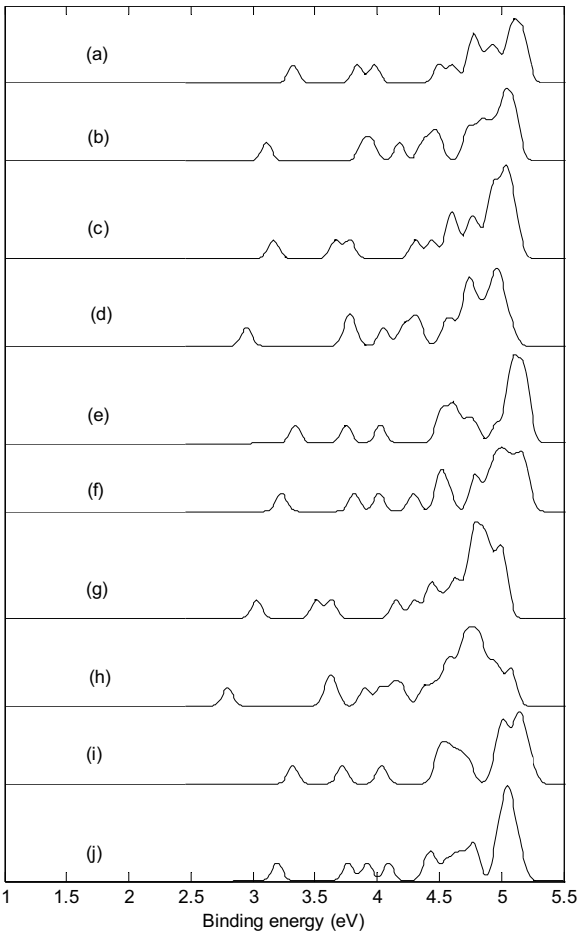

Figure 3. Simulated photoelectron spectra of metalloborospherenes MB_{44}^- (M = Li, Na, and K) based on PBE0 functional with 6–311 + G* basis set. (**a**): C_s Li&B_{44}^- (**I**), (**b**): C_1 Li&B_{44}^- (**IV**), (**c**): C_s Na&B_{44}^- (**I**), (**d**): C_1 Na&B_{44}^- (**IV**), (**e**): C_{2v} Na@B_{44}^- (**I**), (**f**): C_2 Na@B_{44}^- (**IV**), (**g**): C_s K&B_{44}^- (**I**), (**h**): C_1 K&B_{44}^- (**IV**), (**i**): C_{2v} K@B_{44}^- (**I**), (**j**): C_2 K@B_{44}^- (**IV**). The simulations were done by fitting the distributions of calculated vertical detachment energies at the PBE0 level with unit-area Gaussian functions of 0.05 eV half-width.

Normal mode frequencies, infrared intensities and Raman activities of $B_{44}^{0/-}$ and metalloborospherenes $MB_{44}^{0/-}$ (M = Li, Na, and K) are calculated and depicted in Figs 4 and 7. Predicted spectral peaks distribute in three regions: low frequency region (from 0 to 600 cm^{-1}), middle frequency region (from 600 to 1000 cm^{-1}) and high frequency region (from 1000 to 1600 cm^{-1}). These vibrational modes within high frequency region are closely related to molecular structure. This suggests that molecular with slightly difference can lead to the subtle differences of infrared absorption in this region, namely, the infrared spectra of molecular show the characteristics of molecular, like fingerprints, known as fingerprint region.

Infrared spectra of borospherenes $B_{44}^{0/-}$ are given in Fig. 4. Figure 4(a) presents the infrared spectrum of B_{44} (**I**), the sharpest peak occurs at 1295 cm^{-1}. In addition, at 143 and 262 cm^{-1}, the characteristic peaks are strong, which is different from other isomers. The two strong peaks are produced by bending vibration of boron atoms and they belong to the far-infrared region. It's worth noting that infrared spectrum of B_{44} (**I**) is somewhat similar to that of borospherene B_{40} except for the two peaks at 143 and 262 cm^{-1}. Figure 4(b) presents the infrared spectrum of B_{44}^- (**I**), the sharpest peak occurs at 1271 cm^{-1}. The computed IR spectra of $B_{44}^{0/-}$ (**I**) indicate that there are some IR inactive modes and only a few of IR active modes have strong absorption. As shown in Fig. 4(a,b), the addition of an electron does not change the symmetry, but leads to an other strong peaks (at 1217 cm^{-1}) in the high frequency region and redshifts the three main peaks from 1295, 262 and 143 cm^{-1} for B_{44} (**I**) to 1271, 241, and 45 cm^{-1} for B_{44}^- (**I**), respectively, which will be useful to identify the anionic B_{44}^- (**I**) and neutral B_{44} (**I**). Figure 4(c–j) present the infrared spectra of $B_{44}^{0/-}$ (**II-V**), the sharpest peaks of B_{44} (**II**), B_{44}^- (**II**), B_{44} (**III**), B_{44}^- (**III**), B_{44} (**IV**), B_{44}^- (**IV**), B_{44} (**V**) and B_{44}^- (**V**) are at 1285, 1274, 1289, 1274, 1262, 1287, 1286 and 1281 cm^{-1}, respectively. The sharpest peaks of these borospherenes $B_{44}^{0/-}$ are at high frequency region. Figure 4(d,f) show that B_{44}^- (**II**) and B_{44}^- (**III**) have almost the same infrared spectrum, however, Fig. 4(c,e) show that B_{44} (**II**) and B_{44} (**III**) have the similar infrared spectra, which further indicates that the two neutral isomers have the similar structures, instead of same structure. The B_{44} (**IV**) has two strong characteristic peaks at 1262 and 1301 cm^{-1}, whereas the addition of an electron weakens the two strong vibrational modes and leads to another strong characteristic peak at 1287 cm^{-1}. These features can be used to distinguish the B_{44} (**IV**) and B_{44}^- (**IV**). Figure 4(a,b,g,h) show that $B_{44}^{0/-}$ (**I**) and $B_{44}^{0/-}$ (**IV**) have different characteristic peaks, which can be used to distinguish $B_{44}^{0/-}$ (**I**) and $B_{44}^{0/-}$ (**IV**).

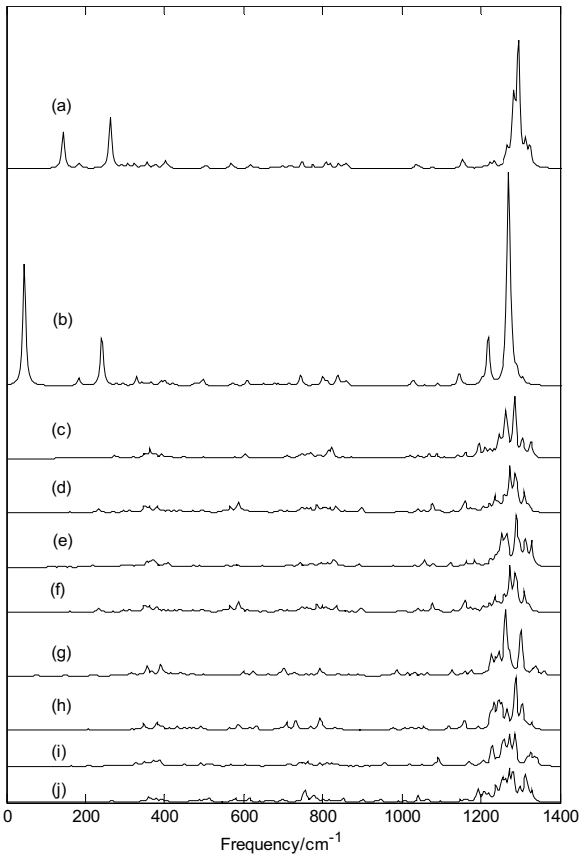

Figure 4. Predicted infrared spectra of $B_{44}^{0/-}$ based on PBE0 functional with 6–311 + G* basis set. (**a**): C_{2v} B_{44} (**I**), (**b**):C_{2v} B_{44}^- (**I**), (**c**): C_1 B_{44} (**II**), (**d**): C_1 B_{44}^- (**II**), (**e**): C_1 B_{44} (**III**), (**f**): C_1 B_{44}^- (**III**), (**g**): C_2 B_{44} (**IV**), (**h**): C_2 B_{44}^- (**IV**), (**i**): C_1 B_{44} (**V**), (**j**): C_1 B_{44}^- (**V**).

Figure 5 shows that the most strong infrared peaks of metalloborospherenes $MB_{44}^{0/-}$ (M = Li, Na, and K) distribute in high-frequency region (from 1000 to 1400 cm^{-1}), and other peaks are relatively weak. Figure 5(a–j) present the infrared spectra of $M\&B_{44}^{0/-}$ (**I**), the sharpest peaks of Li&B_{44} (**I**), Li&B_{44}^- (**I**), Na&B_{44} (**I**), Na&B_{44}^- (**I**), Na@B_{44} (**I**), Na@B_{44}^- (**I**), K&B_{44} (**I**), K&B_{44}^- (**I**), K@B_{44} (**I**) and K@B_{44}^- (**I**) are at 1274, 1272, 1272, 1271, 1286, 1264, 1270, 1270, 1281 and 1241 cm^{-1}, respectively. The sharpest peaks of metalloborospherenes $MB_{44}^{0/-}$ (M = Li, Na, and K) are at high frequency region, and these vibrational modes formed by stretching vibrations of boron atoms. Figure 5(a–d,g,h) show that exohedral $M\&B_{44}^{0/-}$ (**I**, M = Li, Na, and K) have similar infrared spectra, but the main peaks of each anionic metalloborospherene are redshifted somewhat since the extra electron modifies the electronic structures. Figure 5(e,f, i,j) present the infrared spectra of endohedral $M@B_{44}^{0/-}$ (**I**, M = Na, and K), and the results show that the addition of an electron weakens some strong vibrational modes and leads to some strong characteristic peaks. Figure 5(k–t) present the infrared spectra of $M\&B_{44}^{0/-}$ (**IV**), the sharpest peaks of Li&B_{44} (**IV**), Li&B_{44}^- (**IV**), Na&B_{44} (**IV**), Na&B_{44}^- (**IV**), Na@B_{44} (**IV**), Na@B_{44}^- (**IV**), K&B_{44} (**IV**), K&B_{44}^- (**IV**), K@B_{44} (**IV**) and K@B_{44}^- (**IV**) are at 1284, 1294, 1285, 1294, 1286, 1234, 1287, 1226, 1297 and 1236 cm^{-1}, respectively. Like the exohedral $M\&B_{44}$ (**I**), Fig. 5(k–n,q,r) show that exohedral $M\&B_{44}$ (**IV**) have the similar infrared spectra. The predicted infrared spectra in Fig. 5 show that metalloborospherenes $M\&B_{44}^{0/-}$ (**IV**) have different spectral features and characteristic peaks compared with the corresponding $M\&B_{44}^{0/-}$ (**I**) such as $M\&B_{44}^{0/-}$ (**I**) contain some vibration modes with higher frequencies.

Infrared spectra of $B_{44}^{0/-}$ (**I**) are different from that of exohedral $M\&B_{44}^{0/-}$ (**I**, M = Li, Na, and K), the metal dopant in $B_{44}^{0/-}$ (**I**) changes the IR spectra of $B_{44}^{0/-}$ (**I**) such as some weakened vibrational modes and some enhanced characteristic peaks. Note that the sharpest peaks of exohedral $M\&B_{44}^{0/-}$ (**I**, M = Li, Na, and K) are located at about 1270 cm^{-1} and are almost same with the location (at 1271 cm^{-1}) of sharpest peak for B_{44}^- (**I**), but the intensity of sharpest peaks for $M\&B_{44}^{0/-}$ (**I**, M = Li, Na, and K) are significantly weakened. Figures 4(a) and 5(e,i) show that the infrared spectra of endohedral Na@B_{44} and K@B_{44} are similar to that of B_{44}, whereas the addition of metal atom weakens some strong vibrational modes and leads to some strong characteristic peaks. It's worth noting that the infrared spectra of exohedral $M\&B_{44}^{0/-}$ (**I**, M = Li, Na, and K) and endohedral $M@B_{44}^-$ (**I**, M = Na, and K) are quite similar to that of dianion B_{44}^{2-} (**I**)(Figure S2). It suggests that B_{44} (**I**) tends to get electrons from the extra electron and the doped metal. As the analysis of $M@B_{40}$ (M = Ca,Sr) and $M\&B_{40}$ (M = Be,Mg)[35], exohedral metalloborospherenes $M\&B_{44}^{0/-}$ (**I**, M = Li, Na, and K) and endohedral $M@B_{44}^-$ (**I**, M = Na, and K) are characterized as charge-transfer complexes ($M^{2+}B_{44}^{2-}$), where metal atom donates one electron or two electrons to B_{44} (**I**), resulting in similar features with anionic B_{44}^{2-} (**I**). Similarly, infrared spectra

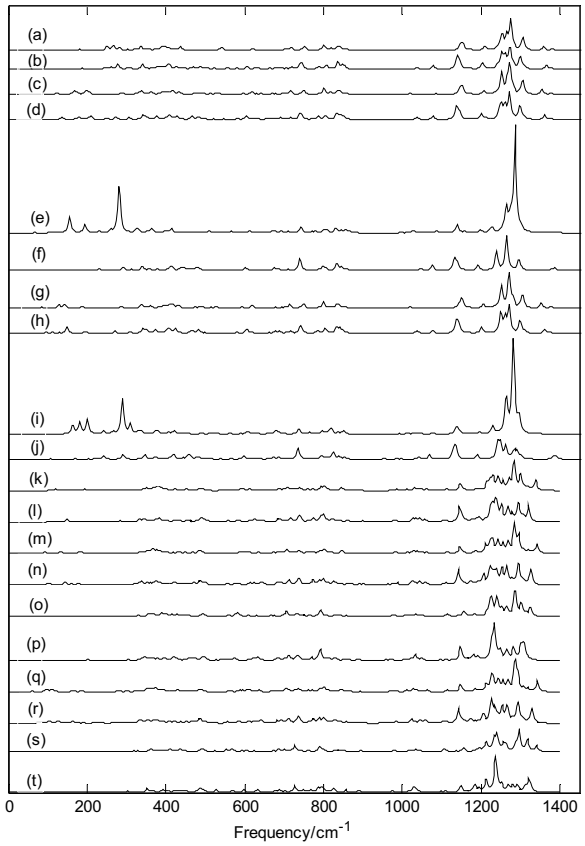

Figure 5. Predicted infrared spectra of metalloborospherenes $MB_{44}^{0/-}$ (M = Li, Na, and K) based on PBE0 functional with 6–311 + G* basis set. (**a**): C_s Li&B_{44} (**I**), (**b**):C_s Li&B_{44}^- (**I**), (**c**): C_s Na&B_{44} (**I**), (**d**): C_s Na&B_{44}^- (**I**), (**e**): C_{2v} Na@B_{44} (**I**), (**f**): C_{2v} Na@B_{44}^- (**I**), (**g**): C_s K&B_{44} (**I**), (**h**): C_s K&B_{44}^- (**I**), (**i**): C_{2v} K@B_{44} (**I**), (**j**): C_{2v} K@B_{44}^- (**I**), (**k**): C_1 Li&B_{44} (**IV**), (**l**):C_1 Li&B_{44}^- (**IV**), (**m**): C_1 Na&B_{44} (**IV**), (**n**): C_1 Na&B_{44}^- (**IV**), (**o**): C_2 Na@B_{44} (**IV**), (**p**): C_2 Na@B_{44}^- (**IV**), (**q**): C_1 K&B_{44} (**IV**), (**r**): C_1 K&B_{44}^- (**IV**), (**s**): C_2 K@B_{44} (**IV**), (**t**): C_2 K@B_{44}^- (**IV**).

of exohedral M&B_{44}^- (**IV**, M = Li, Na, and K) and endohedral M@B_{44}^- (**IV**, M = Na, and K) are somewhat similar to that of dianion B_{44}^{2-} (**IV**) (Figure S2). It suggests that the extra electron moves to B_{44} (**IV**) and the doped metal donates one electron to B_{44} (**IV**), resulting in similar features with anionic B_{44}^{2-}(**IV**). However, exohedral M&B_{44} (**IV**, M = Li, Na, and K) and endohedral M@B_{44} (**IV**, M = Na, and K) are somewhat similar to that of anion B_{44}^- (**IV**). It suggests that B_{44} (**IV**) tends to get one electron from the doped metal. The predicted infrared spectra also provide some information for the identification of B_{44}^- and metalloborospherenes MB_{44}^- (M = Li, Na, and K), these different characteristic peaks provide a theoretical basis for the identification and confirmation of B_{44}^- and metalloborospherenes $MB_{44}^{0/-}$ (M = Li, Na, and K).

Figure 6 depicts the Raman spectra of $B_{44}^{0/-}$. Figure 6(a) depicts the Raman spectrum of B_{44} (**I**), the sharpest peak occurs at 1312 cm^{-1}. Among the Raman active modes, the vibration at 144 cm^{-1} belongs to typical radial breathing mode, which is similar to the typical radial breathing mode of B_{40}[47] at 170 cm^{-1}. The breathing modes are used to identify the hollow structures in nanotubes. Figure 6(b) depicts the Raman spectrum of B_{44}^- (**I**), the sharpest peak occurs at 1307 cm^{-1}. Similar to B_{44} (**I**), the vibration at 139 cm^{-1} belongs to typical radial breathing mode, which is similar to the typical radial breathing mode of B_{40}^- [43] at 176 cm^{-1}. Figure 6(b) indicates that there are four main Raman peaks in the high frequency region and some strong Raman peaks in the middle and lower frequency regions. It's worth noting that the Raman spectrum of B_{44}^- (**I**) is far stronger than that of other $B_{44}^{0/-}$. The computed Raman spectra of $B_{44}^{0/-}$ (**I**) suggest that all vibration modes are Raman active modes, but only a few of them have strong Raman activity. Figure 6(c–j) depict the Raman spectra of $B_{44}^{0/-}$ (**II**-**V**), the sharpest peaks for B_{44} (**II**), B_{44}^- (**II**), B_{44} (**III**), B_{44}^- (**III**), B_{44} (**IV**), B_{44}^- (**IV**), B_{44} (**V**) and B_{44}^- (**V**) are at 1329, 1321, 1327, 1321, 1344, 1328, 1335 and 1329 cm^{-1}, respectively. The sharpest Raman peaks of $B_{44}^{0/-}$ are at high frequency region, and these vibrational modes are formed by stretching vibration of boron atoms. Figure 6(d,f) show that B_{44}^- (**II**) and B_{44}^- (**III**) have almost the same Raman spectrum, however, Fig. 6(c,e) show that B_{44} (**II**) and B_{44} (**III**) have the similar Raman spectra. It further indicates that the two neutral isomers have the similar structures and the two anionic isomers have almost the same structure. Figure 6 indicates that the addition of an electron leads to the redshift of sharpest peak for each isomer. In addition, the calculated results indicate that all vibrational modes of $B_{44}^{0/-}$ (**II**), $B_{44}^{0/-}$ (**III**), $B_{44}^{0/-}$ (**IV**) and $B_{44}^{0/-}$ (**V**) are infrared active and Raman active, however, some vibrational modes of $B_{44}^{0/-}$ (**I**) are infrared inactive. The relatively high symmetric structure (C_{2v}) of $B_{44}^{0/-}$ (**I**) may lead to the infrared inactive vibrational modes.

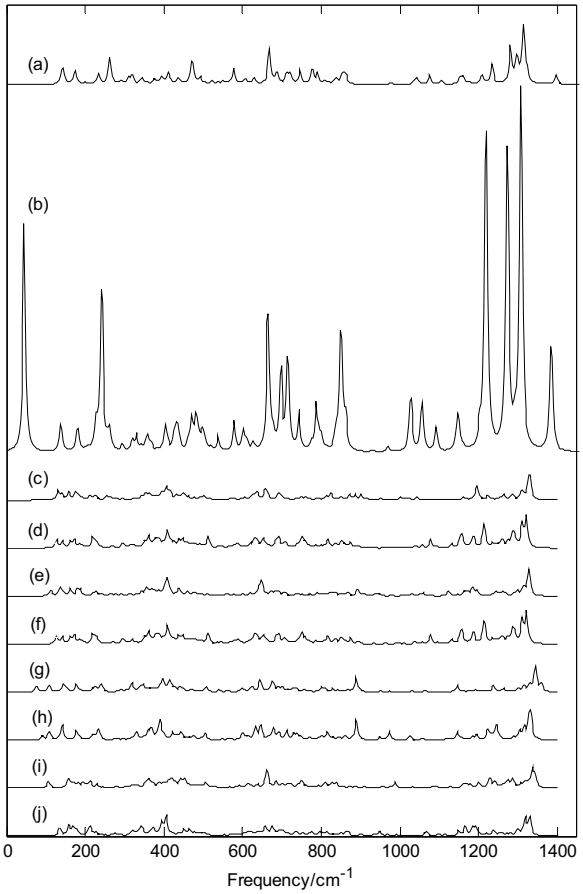

Figure 6. Predicted Raman spectra for the 5 isomers of $B_{44}^{0/-}$ based on PBE0 functional with 6–311 + G* basis set. (**a**): C_{2v} B_{44} (**I**), (**b**): C_{2v} B_{44}^{-} (**I**), (**c**): C_1 B_{44} (**II**), (**d**): C_1 B_{44}^{-} (**II**), (**e**): C_1 B_{44} (**III**), (**f**): C_1 B_{44}^{-} (**III**), (**g**): C_2 B_{44} (**IV**), (**h**): C_2 B_{44}^{-} (**IV**), (**i**): C_1 B_{44} (**V**), (**j**): C_1 B_{44}^{-} (**V**).

Figure 7 depicts the Raman spectra of metalloborospherenes $MB_{44}^{0/-}$ (M = Li, Na, and K). Figure 7(a–j) depict the Raman spectra of M&B_{44} (**I**, M = Li, Na, and K), the sharpest peaks for Li&B_{44} (**I**), Li&B_{44}^{-} (**I**), Na&B_{44} (**I**), Na&B_{44}^{-} (**I**), Na@B_{44} (**I**), Na@B_{44}^{-} (**I**), K&B_{44} (**I**), K&B_{44}^{-} (**I**), K@B_{44} (**I**) and K@B_{44}^{-} (**I**) are at 1361, 1314, 1356, 1314, 1305, 1305, 1355, 1313, 1302 and 1303 cm^{-1}, respectively. The calculated results indicate that all vibrational modes of Li&$B_{44}^{0/-}$ (**I**), Na&$B_{44}^{0/-}$ (**I**) and K&B_{44} (**I**) are infrared active and Raman active, however, some vibrational modes of K&B_{44}^{-} (**I**), Na@$B_{44}^{0/-}$ (**I**) and K@$B_{44}^{0/-}$ (**I**) are infrared inactive. Figure 7(a–d,g,h) depict the Raman spectra of exohedral M&$B_{44}^{0/-}$ (**I**, M = Li, Na, K), they have the similar spectral features. Figure 7(a,c,g) show that exohedral M&B_{44} (**I**, M = Li, Na, and K) have almost the same Raman spectrum, and Fig. 7(b,d,h) show that exohedral M&B_{44}^{-} (**I**, M = Li, Na, and K) have almost the same Raman spectrum. Interestingly, the addition of an electron blueshifts the first two strong peaks and reverses the intensity of first two strong peaks. Figure 7(e,i) show that endohedral Na@B_{44} (**I**) and K@B_{44} (**I**) have the similar Raman spectra, and Fig. 7(f,j) show that endohedral Na@B_{44}^{-} (**I**) and K@B_{44}^{-} (**I**) have the similar Raman spectra. Figure 7(e,f, i,j) show that the addition of an electron weakens some strong characteristic peaks. Figure 7(k–t) depict the Raman spectra of M&B_{44} (**IV**, M = Li, Na, and K), the sharpest peaks of Li&B_{44} (**IV**), Li&B_{44}^{-} (**IV**), Na&B_{44} (**IV**), Na&B_{44}^{-} (**IV**), Na@B_{44} (**IV**), Na@B_{44}^{-} (**IV**), K&B_{44} (**IV**), K&B_{44}^{-} (**IV**), K@B_{44} (**IV**) and K@B_{44}^{-} (**IV**) are at 1334, 1321, 1334, 1320, 1332, 1321, 1333, 1320, 1319 and 1321 cm^{-1}, respectively. Figure 7(k–r) indicate that the addition of an electron leads to the redshift of sharpest peak.

Figures 6 and 7 indicate that doping of metal atom in $B_{44}^{0/-}$ (**I**, **IV**) changes the Raman peaks of $B_{44}^{0/-}$ (**I**, **IV**) such as some weakened vibrational modes and some enhanced characteristic peaks. It's worth noting that the Raman spectra of exohedral M&$B_{44}^{0/-}$ (**I**, M = Li, Na, and K) and endohedral M@B_{44}^{-} (**I**, M = Na, and K) are similar to that of dianion B_{44}^{2-} (Figure S3). It further suggests that B_{44} (**I**) tends to get electrons from the extra electron and the doped metal. Exohedral metalloborospherenes M&$B_{44}^{0/-}$ (**I**, M = Li, Na, and K) and endohedral M@B_{44}^{-} (**I**, M = Na, and K) are characterized as charge-transfer complexes ($M^{2+}B_{44}^{2-}$), where metal atom donates one electron or two electrons to B_{44}(**I**), resulting in similar features with anionic B_{44}^{2-}(**I**). Like the infrared spectra of metalloborospherenes M&B_{44}^{-} (**IV**, M = Li, Na, and K), Raman spectra of exohedral M&B_{44}^{-} (**IV**, M = Li, Na, and K) and endohedral M@B_{44}^{-} (**IV**, M = Na, and K) are somewhat similar to that of dianion B_{44}^{2-} (**IV**) (Figure S3), it further suggests that B_{44} (**IV**) tends to get two electrons from the extra electron and the doped metal, respectively. Raman spectra, as the supplement of infrared spectra, can also be used for the basis of identification of $B_{44}^{0/-}$ and metalloborospherenes $MB_{44}^{0/-}$ (M = Li, Na, and K). From the infrared and Raman

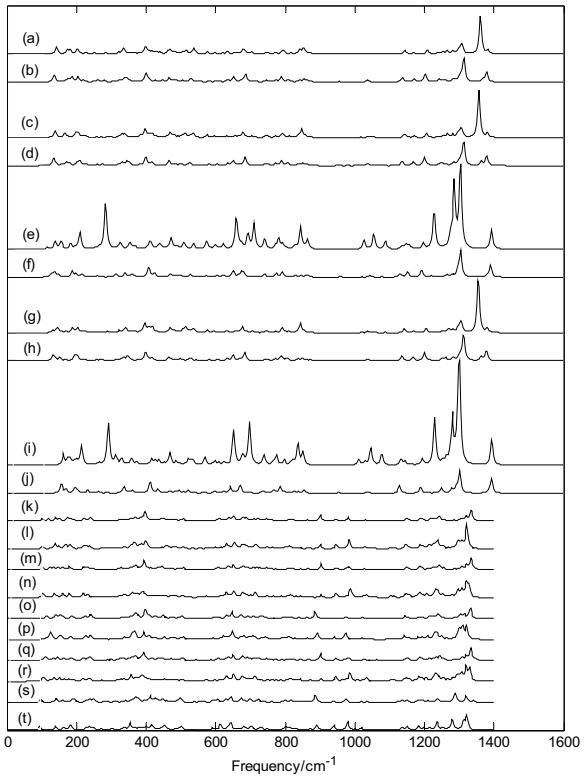

Figure 7. Predicted Raman spectra of metalloborospherenes $MB_{44}^{0/-}$ (M = Li, Na, and K) based on PBE0 functional with 6–311 + G* basis set. (**a**): C_s Li&B_{44} (**I**), (**b**): C_s Li&B_{44}^- (**I**), (**c**): C_s Na&B_{44} (**I**), (**d**): C_s Na&B_{44}^- (**I**), (**e**): C_{2v} Na@B_{44} (**I**), (**f**): C_{2v} Na@B_{44}^- (**I**), (**g**): C_s K&B_{44} (**I**), (**h**): C_s K&B_{44}^- (**I**), (**i**): C_{2v} K@B_{44} (**I**), (**j**): C_{2v} K@B_{44}^- (**I**), (**k**): C_1 LiB_{44} (**IV**), (**l**): C_1 LiB_{44}^- (**IV**), (**m**): C_1 Na&B_{44} (**IV**), (**n**): C_1 Na&B_{44}^- (**IV**), (**o**): C_2 Na@B_{44} (**IV**), (**p**): C_2 Na@B_{44}^- (**IV**), (**q**): C_1 K&B_{44} (**IV**), (**r**): C_1 K&B_{44}^- (**IV**), (**s**): C_2 K@B_{44} (**IV**), (**t**): C_2 K@B_{44}^- (**IV**).

spectra of each borospherene or metalloborospherene, we can find, at some frequencies, infrared absorption peaks are strong, but the Raman peaks are very weak. However, at some frequencies, the relation is just opposite. In addition, at some frequencies, both the infrared and Raman peaks are strong. A vibrational mode of molecular with no change of dipole moment is infrared inactive, we can't obtain the normal mode frequency from the infrared spectral data in experiments. However, this vibrational mode may lead to the change of polarizability, this indicates that the vibrational mode is Raman active. The calculated Raman spectra can be useful for analytical purposes and contribute significantly to spectral interpretation and vibrational assignments, also can provide technical guidance for future synthesis.

Finally, we calculated electronic absorption spectra of B_{44} and metalloborospherenes MB_{44}^- (M = Li, Na, K) with closed-shell electronic structure, as shown in Fig. 8. Figure 8(a–e) present the electronic absorption spectra of B_{44} (**I**, **II**, **III**, **IV**, and **V**), the calculated strongest absorption peaks and the largest excitation wavelengths of B_{44} (**I**, **II**, **III**, **IV**, and **V**) are at 485, 460 472, 622 and 446 nm and 1730, 1207, 913 1247 and 720 nm, respectively. Note that the oscillator strength of largest excitation wavelength for isomer **IV** is zero, and the largest excitation wavelength (with small oscillator strength) is 1035 nm. The minimum excitation energy (the largest excitation wavelength) mainly comes from the electron transition from HOMO to LUMO. HOMO–LUMO energy gap reflects the probability of the molecules jumping from ground state to excited state. Generally speaking, the larger energy gap can lead to the larger electron excitation energy, i.e., the smaller the probability of electronic transition. On the contrary, the molecule with smaller energy gap is easier to jump to the excited state. According to the previous results, the HOMO–LUMO energy gaps are 1.35, 1.85, 2.12, 2.24 and 2.59 eV for B_{44} (**I**), B_{44} (**II**), B_{44} (**IV**), B_{44} (**III**) and B_{44} (**V**), respectively. Although the energy gap of ground state does not represent the minimum excitation energy, the increasing HOMO–LUMO energy gaps just reflect the decreasing largest excitation wavelengths 1730, 1207, 1035, 913, and 720 nm for B_{44} (**V**), B_{44}(**III**), B_{44} (**IV**), B_{44}(**II**) and B_{44} (**I**), respectively. Figure 8(a–e) indicate that electronic absorption spectrum of B_{44} (**I**) is apparently red-shifted comparing with other isomers.

Figure 8(f–j) present the electronic absorption spectra of metalloborospherenes MB_{44}^- (**I**), the calculated largest excitation wavelengths of Li&B_{44}^- (**I**), Na&B_{44}^- (**I**), Na@B_{44}^- (**I**), K&B_{44}^- (**I**) and K@B_{44}^- (**I**) are at 1048, 1057, 1112 1044 and 1118 nm, respectively. However, the oscillator strength of the largest excitation wavelengths of Li&B_{44}^- (**I**), Na@B_{44}^- (**I**) and K&B_{44}^- (**I**) are zero, and the largest excitation wavelengths (with small oscillator strength) for them are at 970, 1084 and 994 nm. The computed results show that Li&B_{44}^- (**I**) and Na&B_{44}^- (**I**) have the similar electronic absorption spectra. Figure 8(k–o) present the electronic absorption spectra of metalloborospherenes MB_{44}^- (**IV**), the calculated largest excitation wavelengths of Li&B_{44}^- (**IV**), Na&B_{44}^- (**IV**), Na@B_{44}^- (**IV**), K&B_{44}^- (**IV**) and K@B_{44}^- (**IV**) are at 1348, 1340, 1392 1353 and 1617 nm, respectively. Figure 8(a–e)

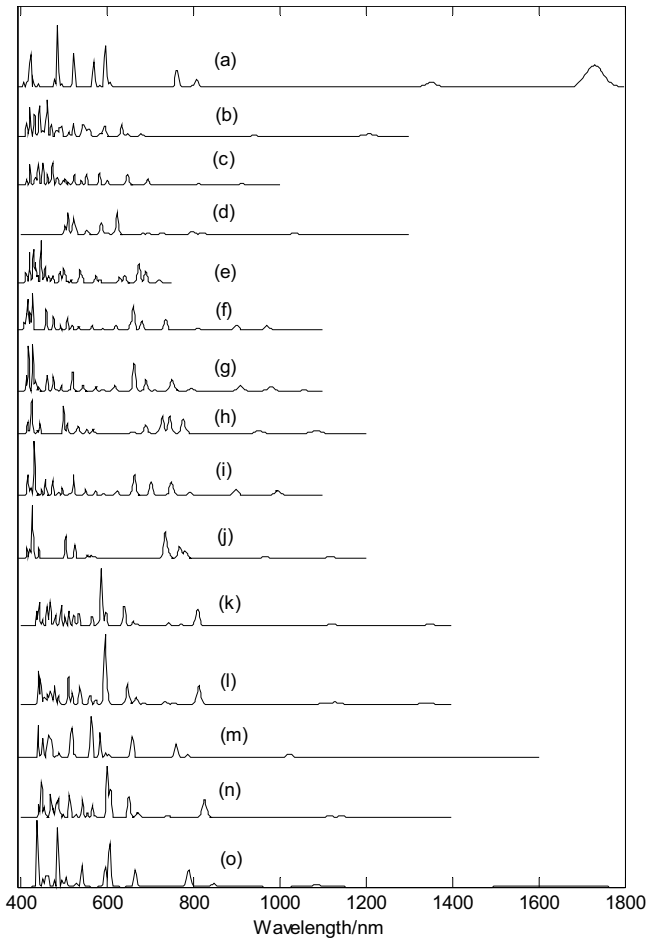

Figure 8. Predicted electronic absorption spectra of B_{44} and metalloborospherenes MB_{44}^- (M = Li, Na, and K) with closed-shell electronic structure based on PBE0 functional with 6–311 + G* basis set. (**a**): C_{2v} B_{44} (**I**), (**b**): C_1 B_{44} (**II**), (**c**): C_1 B_{44} (**III**), (**d**): C_2 B_{44} (**IV**), (**e**): C_1 B_{44} (**V**), (**f**): C_s Li&B_{44}^- (**I**), (**g**): C_s Na&B_{44}^- (**I**), (**h**): C_{2v} Na@B_{44}^- (**I**), (**i**): C_s K&B_{44}^- (**I**), (**j**): C_{2v} K@B_{44}^- (**I**), (**k**): C_1 Li &B_{44}^- (**IV**), (**l**): C_1 Na&B_{44}^- (**IV**), (**m**): C_2 Na@ B_{44}^- (**IV**), (**n**): C_1 K&B_{44}^- (**IV**), (**o**): C_2 K@B_{44}^- (**IV**).

indicate that the largest excitation wavelengths of B_{44} (except for **V**) are in the near infrared region. One can observe several near infrared (NIR) absorption peaks of the B_{44} (**I**, **II**, **III**, and **IV**), whereas B_{44} (**V**) has only UV-Vis absorption peaks. Figure 8(f–o) indicate that the largest excitation wavelengths of metalloborospherenes MB_{44}^- (M = Li, Na, and K) are in the near infrared region. One can observe several near infrared (NIR) absorption peaks of metalloborospherenes MB_{44}^- (M = Li, Na, and K).

Figure 8(a) and (f–j) indicate that doping of metal atom in B_{44} (**I**) blueshifts the largest excitation wavelength since doping of metal atom in B_{44} (**I**) leads to the increase of energy gap (as shown in Tables 1–2). However, Fig. 8(d) and 8(k–o) indicate that doping of metal atom in B_{44} (**IV**) redshifts the largest excitation wavelength since doping of metal atom in B_{44} (**IV**) leads to the decrease of energy gap (as shown in Tables 1–2). It's worth noting that the electronic absorption spectra of exohedral M&B_{44}^- (**I**, M = Li, Na, and K) and endohedral M@B_{44}^- (**I**, M = Na, and K) are similar to that of dianion B_{44}^{2-} (**I**) (Figure S4). Similarly, the electronic absorption spectra of exohedral M&B_{44}^- (**IV**, M = Li, Na, and K) and endohedral M@B_{44}^- (**IV**, M = Na, and K) are similar to that of dianion B_{44}^{2-} (**IV**) (Figure S4). It further suggests that B_{44} (**I**, **IV**) tend to get two electrons from the extra electron and the doped metal, respectively. The electronic absorption spectra may be used for the structural analysis in conjunction with other techniques. In addition, UV-Vis spectroscopy can be used to distinguish isomers, such as the five isomers of B_{44} with obvious different absorption peaks.

In a summary, the structures, stabilities, photoelectron spectra, infrared spectra, Raman spectra, and electronic absorption spectra of B_{44}^- and metalloborospherenes $MB_{44}^{0/-}$ (M = Li, Na, and K) were studied at the level of density functional theory (DFT) and time-dependent density functional theory (TD-DFT) with 6–311 + G* basis set. The calculated results suggest that Li, Na and K atoms can form stable exohedral M&$B_{44}^{0/-}$ (M = Li, Na, and K), whereas only Na and K atoms can be stably encapsulated inside the $B_{44}^{0/-}$ cage. In addition, relative energies of these metalloborospherenes reveal that the Na and K atoms favor the exohedral configuration. More importantly, the addition of metal atom can modify the stability of B_{44} with different structures, which provides a possible route (doping of metal atoms) to produce stable boron clusters or metalloborospherenes. The calculated

results suggest that B_{44} tends to get electrons from the doped metal. Metalloborospherenes MB_{44}^- are characterized as charge-transfer complexes ($M^{2+}B_{44}^{2-}$), where B_{44} tends to get two electrons from the extra electron and the doped metal, resulting in similar features with anionic B_{44}^{2-}. The calculated results show that B_{44}^- and metalloborospherenes $MB_{44}^{0/-}$ (M = Li, Na, and K) have different and meaningful spectral features, insight into the spectral properties is important to understand them and find their potential applications. In addition, the calculated electronic absorption spectra indicate that B_{44} and metalloborospherenes MB_{44}^- (M = Li, Na, and K) have obvious near-IR absorption peaks. These spectral features can be used as fingerprints to identify and distinguish the borospherenes $B_{44}^{0/-}$ and metalloborospherenes $MB_{44}^{0/-}$ (M = Li, Na, and K). The all-boron fullerenes and metalloborospherenes have provided an important clue for the development of new boron-based materials. In view of the remarkable structures and properties, it is possible that borospherenes and metalloborospherenes have potential applications in energy, environment, optoelectronic materials and pharmaceutical chemistry.

References

1. Kroto, H. W. *et al.* C60: buckminsterfullerene. *Nature* **318,** 162–163 (1985).
2. Iijima, S. Helical microtubules of graphitic carbon. *Nature* **354,** 56–58 (1991).
3. Novoselov, K. S. *et al.* Electric Field Effect in Atomically Thin Carbon Films. *Science* **306,** 666–669 (2004).
4. Wang, X.-S. *et al.* Fabrication of Ultralong and Electrically Uniform Single-Walled Carbon Nanotubes on Clean Substrates. *Nano Lett*. **9,** 3137–3141 (2009).
5. Zhu, C.-B. & Wang, X.-L. Tuning the conductance of $H_2O@C_{60}$ by position of the encapsulated H_2O. *Sci*. *Rep*. **5,** 17932 (2015)
6. Kurotobi, K. & Murata, Y. A single molecule of water encapsulated in fullerene C_{60}. *Science* **333,** 613–616 (2011).
7. Tellgmann, R. *et al.* Endohedral Fullerene Production. *Nature* **382,** 407−408 (1996).
8. Okada, H. *et al.* Preparation of endohedral fullerene containing lithium ($Li@C_{60}$) and isolation as pure hexafluorophosphate salt ($[Li^+@C_{60}][PF_6^-]$). *RSC Advances* **2,** 10624–10631 (2012).
9. Suetsuna, T. *et al.* Separation of $N_2@C_{60}$ and $N@C_{60}$. *Chem*. *Eur*. *J*. **8,** 5079–5083 (2002).
10. Li, Y. J. *et al.* Comparison of Nuclear Spin Relaxation of $H_2O@C_{60}$ and $H_2@C_{60}$ and Their Nitroxide Derivatives. *J*. *Phys*. *Chem*. *Lett*. **3,** 1165−1168 (2012).
11. Noguchi, Y., Sugino, O., Okada, H. & Matsuo, Y. First-Principles Investigation on Structural and Optical Properties of $M^+@C_{60}$ (Where M = H, Li, Na, and K). *J*. *Phys*. *Chem*. *C* **117,** 15362–15368 (2013).
12. Zhai, H.-J. *et al.* Hydrocarbon analogues of boron clusters – planarity, aromaticity, and antiaromaticity. *Nature Mater*. **2,** 827–833 (2003).
13. Popov, I. A. *et al.* A combined photoelectron spectroscopy and ab initio study of the quasi-planar B_{24}^- cluster. *J*. *Chem*. *Phys*. **139,** 144307 (2013).
14. Piazza, Z.-A. *et al.* Planar hexagonal B_{36} as a potential basis for extended single-atom layer boron sheets. *Nature Commun*. **5,** 3113 (2014).
15. Sergeeva, A. P. *et al.* Photoelectron Spectroscopic and Theoretical Study of B_{16}^- and B_{16}^{2-}: An All-Boron Naphthalene. *J*. *Am*. *Chem*. *Soc*. **130,** 7244–7246 (2008).
16. Li, W.-L. *et al.* The B_{35} Cluster with a Double-Hexagonal Vacancy: A New and More Flexible Structural Motif for Borophene. Journal of the American Chemical Society. *J*. *Am*. *Chem*. *Soc*. **136,** 12257−12260 (2014).
17. Oger, E. *et al.* Boron Cluster Cations: Transition from Planar to Cylindrical Structures. *Angew*. *Chem*. *Int*. *Ed*. **46,** 8503–8506 (2007).
18. Alexandrova, A. N. *et al.* All-Boron Aromatic Clusters as Potential New Inorganic Ligands and Building Blocks in Chemistry. *Coord*. *Chem*. *Rev*. **250,** 2811–2866 (2006).
19. Sergeeva, A. P. *et al.* Understanding Boron through Size-Selected Clusters: Structure, Chemical Bonding, and Fluxionality. *Acc*. *Chem*. *Res*. **47,** 1349–1358 (2014).
20. Szwacki, N. G., Sadrzadeh, A. & Yakobson, B. I. B_{80} fullerene: An ab initio prediction of geometry, stability, and electronic structure. *Phys*. *Rev*. *Lett*. **98,** 166804–166807 (2007).
21. Zhao, J.-J., Wang, L. Li, F.-Y. & Chen, Z.-F. B_{80} and Other Medium-Sized Boron Clusters: Core−Shell Structures, Not Hollow Cages. *J*. *Phys*. *Chem*. *A* **114,** 9969–9972 (2010).
22. De, S. *et al.* Energy Landscape of Fullerene Materials: A Comparison of Boron to Boron Nitride and Carbon. *Phys*. *Rev*. *Lett*. **106,** 225502 (2011).
23. Sheng, X.-L., Yan, Q.-B., Zheng, Q.-R. & Su, G. Boron fullerenes B_{32+8k} with four-membered rings and B_{32} solid phases:geometrical structures and electronic properties. *Phys*. *Chem*. *Chem*. *Phys*. **11,** 9696–9702 (2009).
24. Wang, L., Zhao, J.-J., Li, F.-Y. & Chen, Z.-F. Boron fullerenes with 32–56 atoms: Irregular cage configurations and electronic properties. *Chem*. *Phys*. *Lett*. **501,** 16–19 (2010).
25. Ozdogan, C. *et al.* The unusually stable B_{100} fullerene, structural transitions in boron nanostructures, and a comparative study of α -and γ-boron and sheets. *J*. *Phys*. *Chem*. *C* **114,** 4362–4375 (2010).
26. Cheng, L.-J. B_{14}: An all-boron fullerene. *J*. *Chem*. *Phys*. **136,** 104301 (2012).
27. Lu, H.-G. & Li, S.-D. Three-chain B6n + 14 cages as possible precursors for the syntheses of boron fullerenes. *J*. *Chem*. **Phys.139,** 224307 (2013).
28. Lv, J., Wang, Y., Zhu, L. & Ma, Y. B_{38}: An all-boron fullerene analogue. *Nanoscale* **6,** 11692–11696 (2014).
29. Zhai, H.-J. *et al.* Observation of an all-boron fullerene. *Nat*. *Chem*. **6,** 727–731 (2014).
30. Chen, Q. *et al.* Experimental and theoretical evidence of an axially chiral borospherene. *ACS Nano* **9,** 754–760 (2015).
31. Martínez-Guajardo, G. *et al.* Dynamical behavior of Borospherene: A Nanobubble. *Sci*. *Rep*. **5,** 11287 (2015).
32. Dong, H.-L. *et al.* New Ti-decorated B_{40} fullerene as a promising hydrogen storage material. *Sci*. *Rep*. **5,** 09952 (2015).
33. Wang, Y.-J. *et al.* Observation and characterization of the smallest borospherene, B_{28}^- and B_{28}. *J*. *Chem*. *Phys*. **144,** 064307 (2016).
34. Li, H.-R. *et al.* Competition between quasi-planar and cage-like structures in the B_{29}^- cluster: photoelectron spectroscopy and ab initio calculations. *Phys*. *Chem*. *Chem*. *Phys*. **18,** 29147–29155 (2016).
35. Bai, H. Chen, Q. Zhai, H.-J. & Li, S.-D. Endohedral and Exohedral Metalloborospherenes: $M@B_{40}$ (M = Ca, Sr) and $M\&B_{40}$ (M = Be, Mg). *Angew*. *Chem*. *Int*. *Ed*. **54,** 941–945 (2015).
36. Jin, P., Hou, Q.-H., Tang, C.-C. & Chen, Z.-F. Computational investigation on the endohedral borofullerenes $M@B_{40}$ (M = Sc, Y, La). *Theor*. *Chem*. *Acc*. **134,** 13 (2015).
37. Fa, W. *et al.* Stability of Metal-Encapsulating Boron Fullerene B_{40}. *J*. *Phys*. *Chem*. *A* **119,** 11208–11214 (2015).
38. Chen, Q. *et al.* Endohedral C_3 $Ca@B_{39}^+$ and C_2 $Ca@B_{39}^+$: axiallychiral metalloborospherenes based on B_{39}^-. *Phys*. *Chem*. *Chem*. *Phys*. **18,** 19690–19694 (2015).
39. Chen, Q. *et al.* Endohedral Ca@B38: stabilization of a B_{38}^{2-} borospherene dianion by metal encapsulation. *Phys*. *Chem*. *Chem*. *Phys*. **18,** 11610–11615 (2016).
40. Chen, Q. *et al.* Endohedral charge-transfer complex $Ca@B_{37}^-$:stabilization of a B_{37}^{3-} borospherene trianion by metal-encapsulation. *Phys*. *Chem*. *Chem*. *Phys*. **18,** 14186–14190 (2016).

41. Tian, W.-J. *et al.* Saturn-like charge-transfer complexes $Li_4\&B_{36}$, $Li_5\&B_{36}^+$, and $Li_6\&B_{36}^{2+}$: exohedral metalloborospherenes with a perfect cage-like B_{36}^{4-} core. *Phys. Chem. Chem. Phys.* **18,** 9922–9926 (2016).
42. He, R.-X. & Zeng, X.-C. Electronic structures and electronic spectra of all-boron fullerene B_{40}. *Chem. Commun.* **51,** 3185–3188 (2015).
43. Li, S.-X. *et al.* Comparative study on the spectral properties of boron clusters $B_n^{0/-1}$ (n = 38–40). *Sci. Rep.* **6,** 25020 (2016).
44. Tai, T.-B. & Nguyen, M. T. A new chiral boron cluster B_{44} containing nonagonal holes. *Chem. Commun.* **52,** 1653 (2016).
45. Bauernschmitt, R. & Ahlrichs, R. Treatment of Electronic Excitations within the Adiabatic Approximation of Time Dependent Density Functional Theory. *Chem. Phys. Lett.* **256,** 454–464 (1996).
46. Frisch, M. J. *et al. Gaussian 09, Revision A.02* (Gaussian Inc., Wallingford, CT, 2009).
47. Chen, Q. *et al.* Cage-like B_{41}^+ and B_{42}^{2+}: New Chiral Members of the Borospherene Family. *Angew. Chem. Int. Ed.* **54,** 8160–8164 (2015).

Acknowledgements

This work is supported by the Guizhou Science & Technology Foundation of China (Grant No. QKH J[2013]2241), the International Science & Technology Cooperation Program of China (Grant No. 2014DFA00670).

Author Contributions

S.L. performed all the calculation work. Z.L. and S.Q. helped in analyzing the results and in writing the manuscript. Z.Z. and S.L. analyzed the results and wrote the manuscript. All authors reviewed the manuscript.

Additional Information

Supplementary information accompanies this paper at http://www.nature.com/srep

Competing financial interests: The authors declare no competing financial interests.

How to cite this article: Li, S. *et al.* Structures, stabilities and spectral properties of borospherene B_{44}^- and metalloborospherenes $MB_{44}^{0/-}$ (M = Li, Na, and K). *Sci. Rep.* **7**, 40081; doi: 10.1038/srep40081 (2017).

Publisher's note: Springer Nature remains neutral with regard to jurisdictional claims in published maps and institutional affiliations.